Solid State Phenomena
ISSN: 1662-9779, Vol. 376, pp 33-40
doi:10.4028/p-MI3pHl

Submitted: 2024-09-20
Revised: 2025-08-05
Accepted: 2025-08-05
Online: 2025-09-10

Dynamics of Stacking Fault Expansion in H^+ Implanted SiC-MOSFETs

Kazuya Ishibashi[1,a*], Naoki Shikama[1,b], Hiroki Niwa[2,c], Takanori Tanaka[1,d], Hiroyuki Amishiro[2,e], Akifumi Imai[2,f], Katsutoshi Sugawara[2,g], Yasuhiro Kagawa[1,h] and Akihiko Furukawa[1,i]

[1]Power Device Works, Mitsubishi Electric Corporation,1-1-1 Imajuku-higashi, Nishi-ku, Fukuoka-shi, Fukuoka, 819-0192, Japan

[2]Advanced Technology R&D Center, Mitsubishi Electric Corporation, 8-1-1 Tsukaguchi-honmachi, Amagasaki-shi, Hyogo, 661-8661, Japan

[a]Ishibashi.Kazuya@ak.mitsubishielectric.co.jp, [b]Shikama.Naoki@df.mitsubishielectric.co.jp, [c]Niwa.Hiroki@dp.mitsubishielectric.co.jp, [d]Tanaka.Takanori@cb.MitsubishiElectric.co.jp, [e]Amishiro.Hiroyuki@cb.mitsubishielectric.co.jp, [f]Imai.Akifumi@ys.MitsubishiElectric.co.jp, [g]Sugawara.Katsutoshi@ea.MitsubishiElectric.co.jp, [h]Kagawa.Yasuhiro@cj.mitsubishielectric.co.jp, [i]Furukawa.Akihiko@df.MitsubishiElectric.co.jp

Keywords: MOSFET, body diode, bipolar degradation, stacking fault, proton implantation

Abstract. Bipolar degradation is a well-known issue when using body diodes in SiC-MOSFETs. Recent studies suggest that H^+ (proton) implantation can effectively inhibit this degradation, but demonstrations on its suppression are still limited. Therefore, in this study, we have experimentally demonstrated how the expansion of Shockley-type stacking faults (SSFs) is suppressed by proton implantation. We fabricated a vertical SiC-MOSFET, in which protons were implanted into the middle depth of the drift layer. We then subjected the body diode to continuous current stress and performed photoluminescence (PL) analysis. Detailed PL image and emission spectral analysis of SSFs revealed that the proton-implanted layer can function as a recombination-enhancing layer during bipolar operation. Furthermore, it can be formed at any depth within the drift layer by controlling the energy, offering a significant advantage in the design of SiC-MOSFETs.

Introduction

Silicon carbide (SiC) is a desirable material for power devices due to its superior properties such as wide bandgap, high critical electric field, and high thermal conductivity. A body diode, which is a parasitic p-n diode within a MOSFET structure, is widely utilized as a free-wheeling diode. By using body diodes, it is possible to reduce costs and achieve miniaturization of systems that comprise SiC power devices, by eliminating the external free-wheeling diode. However, when using the body diode in SiC-MOSFETs, bipolar degradation is a key issue that needs to be considered. The recombination of electron-hole pairs during bipolar operation can lead to the expansion of Shockley-type stacking faults (SSFs), which can lead an increase in forward voltage, on-resistance [1-3], and/or drain-source leakage current. A well-known method for preventing the bipolar degradation is the growth of a highly nitrogen-doped epitaxial layer, which serves as a recombination-enhancing buffer within the drift layer [4]. On the other hand, in recent years, H^+ (proton) implantation has been reported to successfully inhibit the expansion of SSFs in SiC [5,6]. This technique could be a promising candidate, however, there are limited reports demonstrating this inhibitory effect. In this work, to gain a more detailed understanding of the suppression mechanism, we conducted a detailed defect analysis of a proton-implanted SiC-MOSFET in which SSFs expanded after the application of current stress.

Experimental Procedure

A vertical SiC-MOSFET was fabricated on a 12 μm thick drift layer, which included a proton-implanted layer, as shown in Fig. 1. The drift layer was grown on a 4°-off 4H-SiC substrate with a diameter of 150 mm. Protons were partially implanted into the middle depth of the drift layer at a dose of 1×10^{13} cm^{-2}, by partially shielding the device's active area using a silicon piece. Figure 2

shows the experimental flow. Proton implantation was performed just after the epitaxial growth. Following device fabrication, dies were cut from the wafer, and a continuous current stress test was carried out on each body diode of all the dies under conditions of 420 A/cm^2 at 150°C for a duration of 2 minutes. Subsequently, a photoluminescence (PL) inspection was performed after removing all materials on the SiC, such as metal/gate electrodes and SiO_2. At last, Burgers vectors of partial dislocations bounding the SSFs were investigated using a transmission electron microscope (TEM) under two-beam excitation conditions, specifically $\boldsymbol{g} = 11\bar{2}0$ and $\bar{2}110$.

PL analysis after applying the current stress revealed multiple shape patterns of SSF expansion, such as triangular and bar-shaped, due to different Burgers vectors [7]. Additionally, there were some dies that were stressed without SSFs. In this paper, we focus on discussing the detailed analysis results of a specific single die, which exhibits bar-shaped SSFs originating from the proton non-implanted region and expanding across the proton-implanted region.

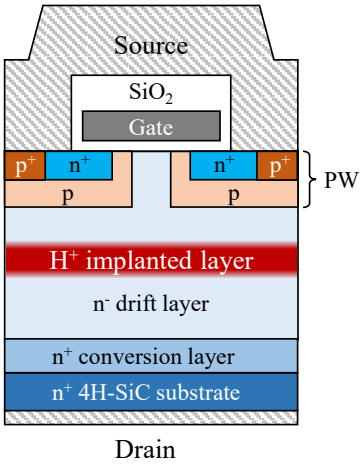

Fig. 1. Cross-sectional schematic diagram of the proton-implanted SiC-MOSFET.

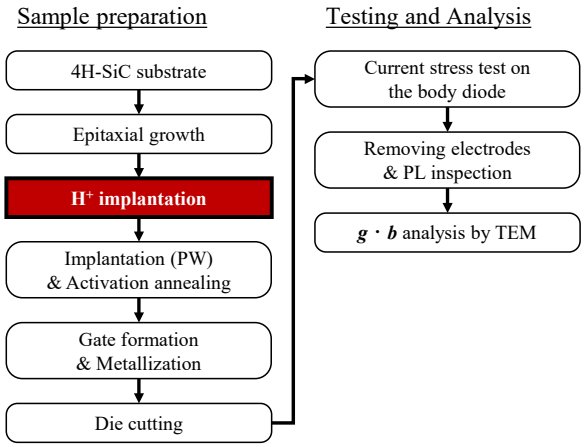

Fig. 2. Experimental flow. The proton implantation was performed just after the epitaxial growth but before the activation annealing.

Results and Discussion

Figures 3(a) and (b) show PL images of the expanded SSFs in the proton-implanted SiC-MOSFET after the continuous current stress test, and Fig. 4 presents a three-dimensional schematic diagram cut along a basal plane that includes specific SSF (**SSF$_1$**). In the PL image taken at $\lambda = 420$ nm shown in Fig. 3(a), two bar-shaped SSFs which exhibit bright emission are observed. Moreover, in Fig. 3(b), Si- and C-core partial dislocations that form the outline of the SSFs can be seen as strong and weak emissions [2], which was taken at the infrared region ($\lambda > 750$ nm). These SSFs (**SSF$_1$** and **SSF$_2$**) on different basal planes appear to overlap along the c-axis ([0001]), as illustrated in the schematic in Fig. 3(c). Both SSFs have their starting points (**a** and **a'**) of expansion in the proton non-implanted region and expand in the $[1\bar{1}00]$ direction. Since carrier recombination mainly occurs in the lightly nitrogen-doped n$^-$ region, the SSF expansion is restricted between the p-well (PW)/drift layer and the drift/conversion layer interfaces, as shown in Fig. 4. In Fig. 3(a), we can see that the SSFs, indicated by the bright contrast, reach the boundary including points **h**, **e**, and **c**, and display a different characteristic feature in the lower region. It is revealed that the SSFs continue to expand even after entering the proton-implanted region. However, the line **e-f** emerges as a dark contrast near the center of the SSFs. This dark region has a width of about 20 μm in the direction of the step flow ($[11\bar{2}0]$), which is the intersection with the SSFs. This width is attributed to the varying depths of the basal planes where **SSF$_1$** and **SSF$_2$** are formed. In this region, two intersection lines with the SSFs for a single proton-implanted layer coexist. Notably, the edge of **SSF$_1$**, including points **h** and **i**, formed an incomplete shape in the left region of the line **e-f**. This region is deeper than the proton-implanted layer in the drift layer. These results suggest that when the expanded SSFs reached the proton-

implanted region, the SSF structure remained unchanged, while the dislocation motion was hindered only in the area deeper than the proton-implanted layer.

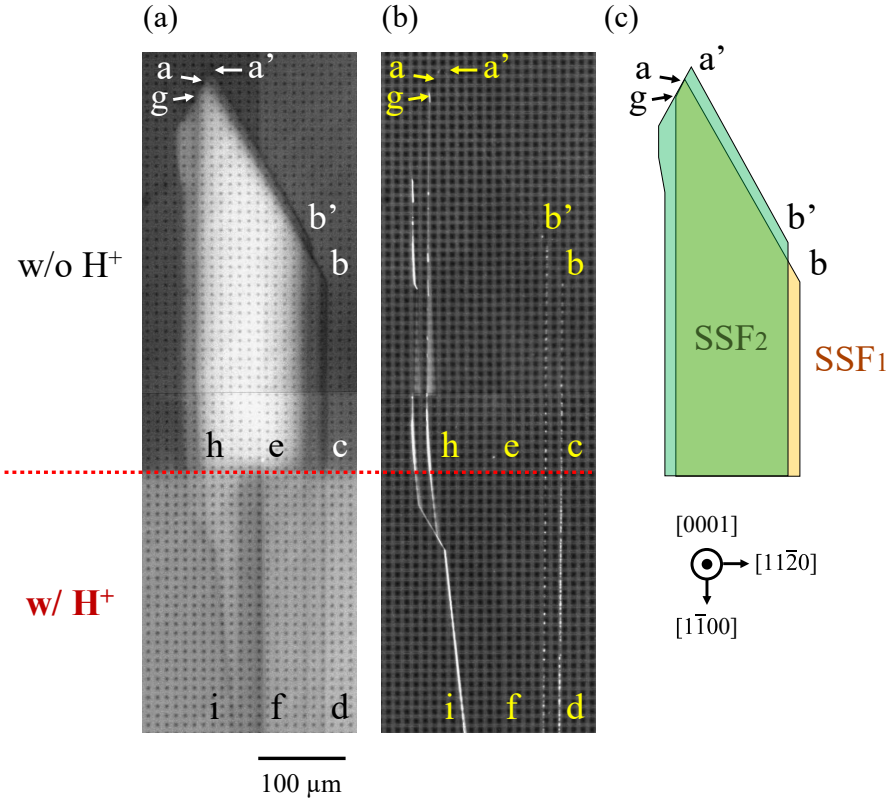

Fig. 3. PL images of the bar-shaped expanded SSFs in the proton-implanted SiC-MOSFET observed with different wavelengths. The wavelengths of the observation filters are (a) λ = 420 nm and (b) λ > 750 nm. (c) Schematic illustration of the two overlapped SSFs on different basal planes, with **a** and **a'** as the respective starting points of expansion.

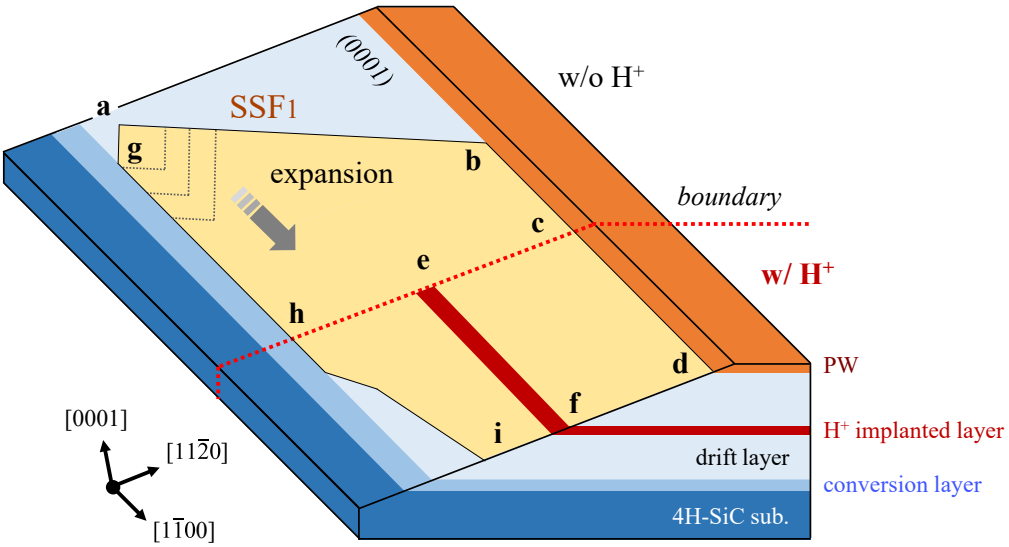

Fig. 4. Three-dimensional schematic diagram of the SSF in the proton-implanted SiC-MOSFET. The specific basal plane, including $\mathbf{SSF_1}$ as discussed in Fig. 3 is shown. The red dashed line shown in the figure indicates the boundary between the proton-implanted region and the proton non-implanted region.

Figure 5(a) shows a planar TEM image of the bar-shaped expanded SSF ($\mathbf{SSF_2}$) in the proton-implanted SiC-MOSFET, taken at near the c-axis ([0001]) incident condition. Figures 5(b) and (c) are planar TEM images taken under different two-beam excitation conditions $\boldsymbol{g}$ =11$\bar{2}$0 and $\bar{2}$110,

respectively. All the images were taken at the same location, which includes the starting point **A** (**a'** in Fig. 3) of the expansion of $\mathbf{SSF_2}$, as shown in the schematic illustration in Fig. 5(d). From these TEM images, it is estimated that $\mathbf{SSF_2}$ is composed of three types of partial dislocations ($\mathbf{PD_{21}}$, $\mathbf{PD_{22}}$ and $\mathbf{PD_{23}}$). These partial dislocations are part of the initial BPD, with $\mathbf{PD_{22}}$ and $\mathbf{PD_{23}}$ expanding after the application of current stress. Conversion of two different threading edge dislocations ($\mathbf{TED_1}$ and $\mathbf{TED_2}$) were confirmed at the end points (**A** and **B**) of $\mathbf{PD_{21}}$. $\mathbf{TED_2}$ is converted from $\mathbf{PD_{21}}$, and $\mathbf{TED_1}$ is converted from $\mathbf{PD_{11}}$ and $\mathbf{PD_{12}}$, which are the partial dislocations bounding $\mathbf{SSF_1}$. Additionally, although the explanation and illustration are omitted, $\mathbf{SSF_1}$ and $\mathbf{SSF_2}$ are expanded from the initial BPDs which have the same type of dislocation structure. $\mathbf{PD_{11}}$ and $\mathbf{PD_{21}}$ are partial dislocations which correspond to the same positions on $\mathbf{SSF_1}$ and $\mathbf{SSF_2}$, respectively. The same applies to $\mathbf{PD_{12}}$ and $\mathbf{PD_{22}}$. The dislocation structure observed in this experiment is similar to the TED-BPD-TED structure reported by Ota *et al*., which is thought to be formed by the conversion from TED to BPD within the drift layer [8]. It is believed that the TED-BPD-TED structure observed in our experiment also formed within the drift layer after epitaxial growth and during the device fabrication process, and that its BPD segment was expanded into the bar-shaped SSF due to the current stress. The Burgers vector of the dislocation can be determined using the contrast rule $\boldsymbol{g} \cdot \boldsymbol{b} = 0$, where the contrast of a dislocation is absent when its Burgers vector $\boldsymbol{b}$ is perpendicular to the $\boldsymbol{g}$ vector. In Fig. 5(b), the contrast of $\mathbf{PD_{12}}$, $\mathbf{PD_{22}}$, and $\mathbf{PD_{23}}$ disappeared at $\boldsymbol{g} = 11\bar{2}0$. In Fig. 5(c), and the contrast of $\mathbf{PD_{11}}$ and $\mathbf{PD_{21}}$ disappeared at $\boldsymbol{g} = \bar{2}110$. From them, Burgers vectors of each partial dislocation were predicted as follows: $\mathbf{PD_{12}}$, $\mathbf{PD_{22}}$, and $\mathbf{PD_{23}}$ have $\boldsymbol{b} = (\pm\, 1/3)\,[1\bar{1}00]$, and $\mathbf{PD_{11}}$ and $\mathbf{PD_{21}}$ have $\boldsymbol{b} = (\pm\, 1/3)\,[0\bar{1}10]$, respectively. Consequently, the structure of the initial BPDs of $\mathbf{SSF_1}$ and $\mathbf{SSF_2}$ were identified as $\boldsymbol{b} = (\pm\, 1/3)\,[1\bar{2}10]$, with a dislocation line direction $\boldsymbol{\zeta} = \pm\,[1\bar{2}10]$.

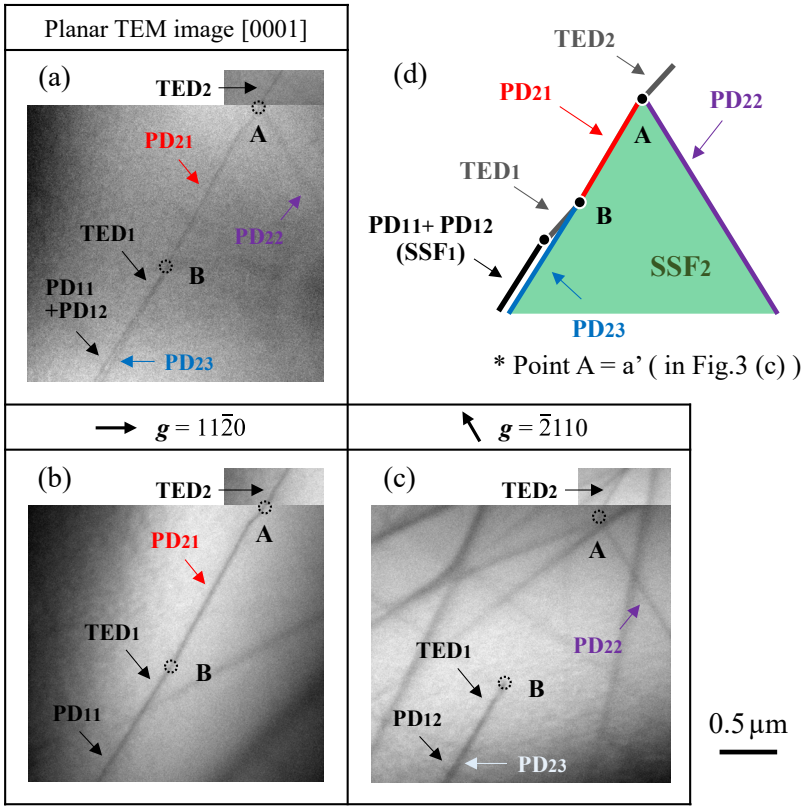

Fig. 5. (a) Planar TEM image at the starting point of expansion of the bar-shaped SSF ($\mathbf{SSF_2}$) in the proton-implanted SiC-MOSFET taken at near the c-axis ([0001]) incident condition. (b), (c) TEM images taken at different two-beam excitation conditions $\boldsymbol{g} = 11\bar{2}0$ and $\bar{2}110$, respectively. (d) Schematic illustration of $\mathbf{SSF_2}$.

It has been reported that when the Burgers vector and dislocation line direction are identified, the expansion pattern of SSF can be uniquely determined from their combination and a type of dislocation loop [9]. In this case, the Burgers vector of the initial BPD was determined from the SSF expansion

pattern as $\boldsymbol{b} = 1/3\,[1\bar{2}10]$, with the dislocation line direction $\boldsymbol{\zeta} = [1\bar{2}10]$. The structures of the initial BPD and SSF are schematically illustrated in Fig. 6.

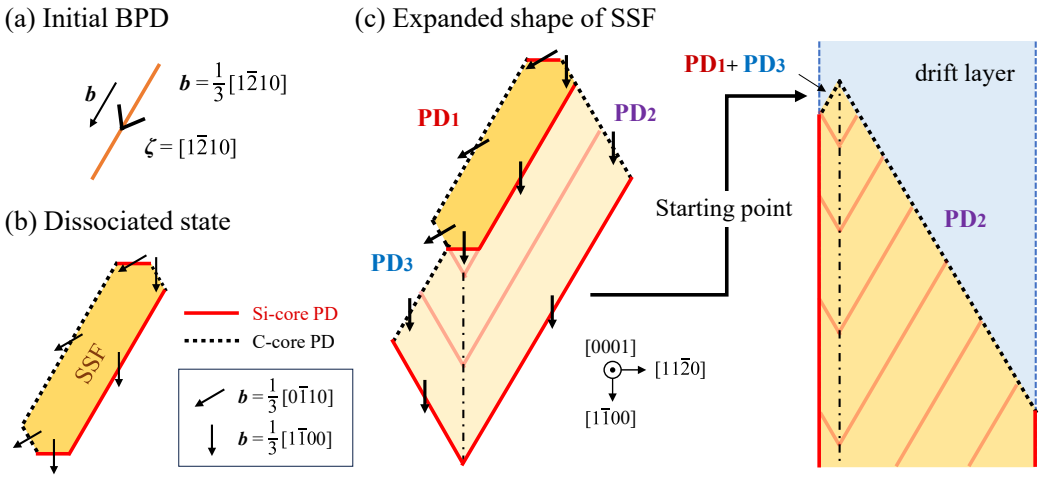

Fig. 6. Schematic illustrations of (a) the initial BPD with Burgers vector $\boldsymbol{b} = 1/3\,[1\bar{2}10]$, and the line direction $\boldsymbol{\zeta} = [1\bar{2}10]$, (b) the dissociated state, and (c) the expanded shape of SSF.

Figures 7(a)-(f) show results of the PL spectra observed in various regions of the proton-implanted SiC-MOSFET. Figures 7(d) and (a) compare the results with and without proton implantation taken at the peripheral area of the MOSFET chip, where no Al ion implantation of the PW has been done. In Fig. 7(d), the PL peak corresponding to the band edge emission of 4H-SiC (λ = 390 nm) decreased, and a broad peak ranging from 420 to 600 nm due to the implantation defects created by proton implantation was observed. Figures 7(e) and (b) compare the results with and without proton implantation in the active area. In Fig. 7(b), a broad peak due to the implantation defects created by Al ion implantation was observed. Interestingly, the broad peaks among the signals shown in Figs. 7(b), (d), and (e) are similar. Although not all defect levels in the band gap exhibit luminescence, these results suggest that some of the same luminescent defect levels were formed during the ion implantations of both Al and H. These are considered to correspond to the point defects that enhance carrier recombination. Figures 7(f) and (c) compare the results with and without proton implantation in the region where the SSFs exist. In Fig. 7(c), a clear peak corresponding to the Single SSF (1SSF) at λ = 420 nm was observed [10]. However, near the intersection of the SSFs and the proton-implanted layer (line **e-f** shown in Figs. 3 and 4), not only was the band edge emission inhibited, but the emission of the SSFs was also suppressed, leading to a reduction in their PL intensities, as shown in Fig. 7(f).

Figure 8 shows the comparison of the PL spectra observed in different regions which include SSFs in the active area of the proton-implanted SiC-MOSFET. The observation points $\mathbf{P_1}$, $\mathbf{P_2}$, and $\mathbf{P_3}$ share the same cross-sectional structure, but the positional relationship between the SSFs and the proton-implanted layer varies in each case, as illustrated in the schematic diagram in Fig. 9. At $\mathbf{P_1}$, the SSFs are located under the proton-implanted layer, while at $\mathbf{P_2}$, they are on the proton-implanted layer, and at $\mathbf{P_3}$, they are near the interface of the PW/drift layer. At $\mathbf{P_1}$, a clear peak corresponding to 1SSF can be observed. However, at both $\mathbf{P_2}$ and $\mathbf{P_3}$, where the stacking faults are in contact with either the proton-implanted layer or the PW, the peak intensities are reduced. This suggests that defect levels, which inhibit recombination of electron-hole pairs and emission at the SSFs, were introduced in the proton implanted layer as well as the PW. From these results, it is inferred that point defects in the drift layer exist at high densities in both implanted layers, as schematically illustrated in Fig. 9. It is estimated that the proton-implanted layer enhances carrier recombination, leading to a lower density of excess carriers in the region deeper than the proton-implanted layer. Based on several reports suggesting that SSFs can contract with fewer injected carriers [11-14], It is hypothesized that the incomplete SSF shape observed deeper than the proton-implanted layer is a result of the contraction of the SSFs. In conclusion, we infer that the proton-implanted layer can function as a recombination-enhancing buffer during the bipolar operation, resulting in suppression of the expansion of SSFs.

Furthermore, it offers a significant advantage in device design of SiC-MOSFETs as this buffer layer can be formed at any depth within the drift layer by controlling the implantation energy.

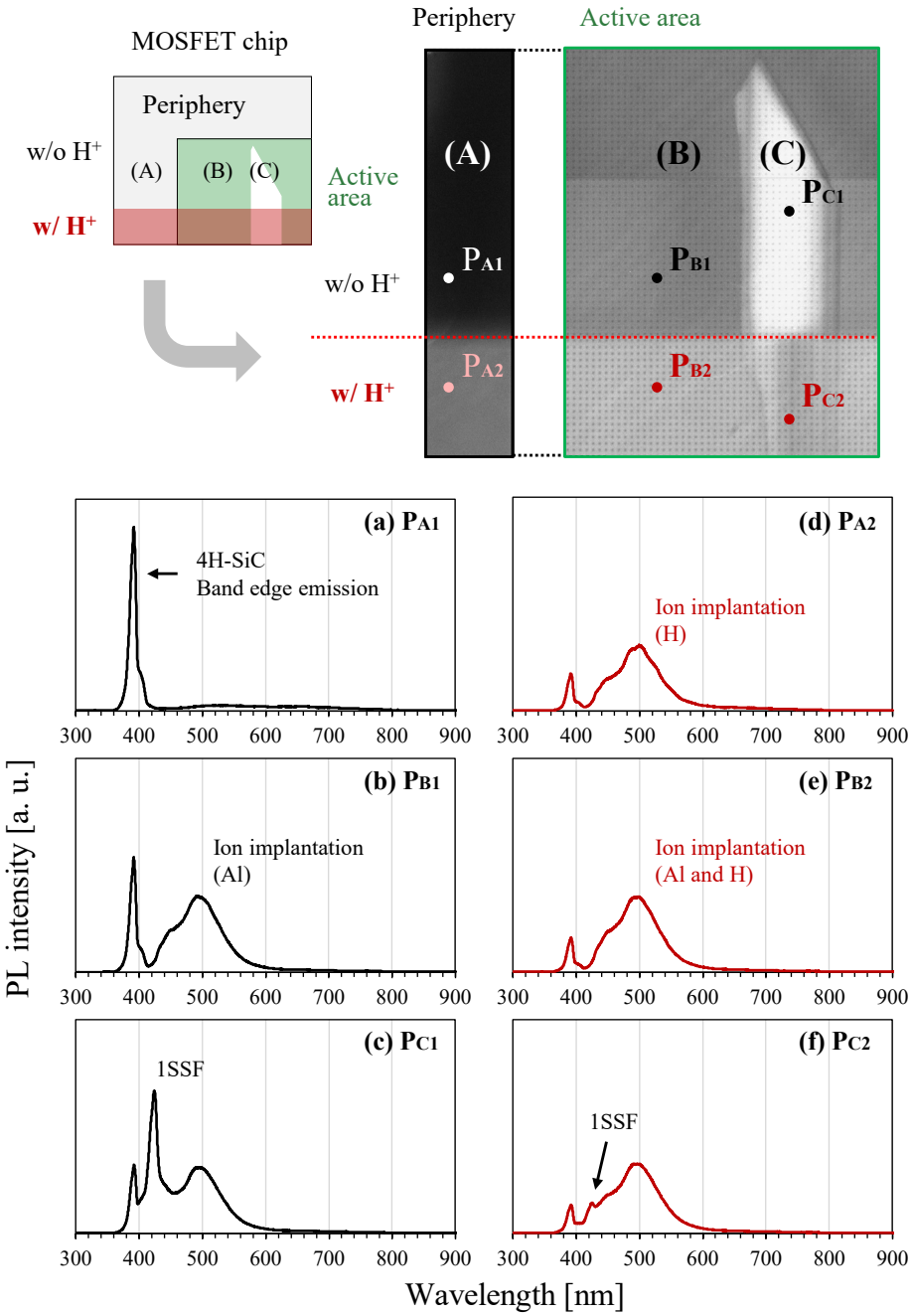

Fig. 7. Comparison of PL spectra observed in various regions of the proton-implanted SiC-MOSFET. (a) $\mathbf{P_{A1}}$, (b) $\mathbf{P_{B1}}$, and (c) $\mathbf{P_{C1}}$ are all observation points within the proton non-implanted region, respectively located at **A**: the peripheral area, **B**: the active area, **C**: the active area with the SSFs.

(d) $\mathbf{P_{A2}}$, (e) $\mathbf{P_{B2}}$, and (f) $\mathbf{P_{C2}}$ are all observation points within the proton-implanted region, each having the same cross-sectional structure as $\mathbf{P_{A1}}$, $\mathbf{P_{B1}}$, and $\mathbf{P_{C1}}$, respectively, except for the presence of the proton-implanted layer in the middle depth of the drift layer. All data were obtained under the identical PL condition excited by He-Cd laser (λ = 325 nm) at room temperature, and the electron-hole pairs created by the excitation light reach almost the entirety of the drift layer.

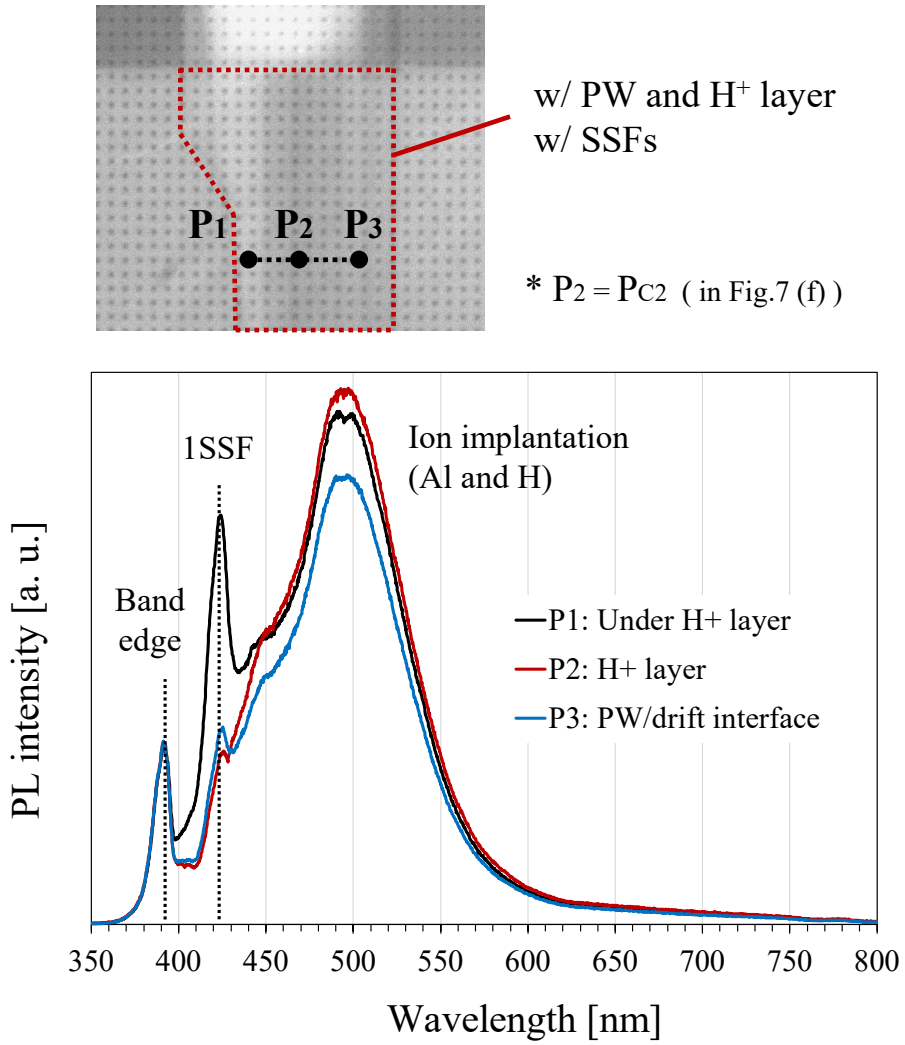

Fig. 8. Comparison of PL spectra observed in different regions with SSFs in the active area of the proton-implanted SiC-MOSFET. In **P1**, **P2**, and **P3**, the positional relationship between the SSFs and the proton-implanted layer in the drift layer varies, as shown in Fig. 9. All data were obtained under the identical PL condition excited by He-Cd laser (λ = 325 nm) at room temperature, and the electron-hole pairs created by the excitation light reach almost the entirety of the drift layer. Each peak intensity is normalized by the peak of the band edge.

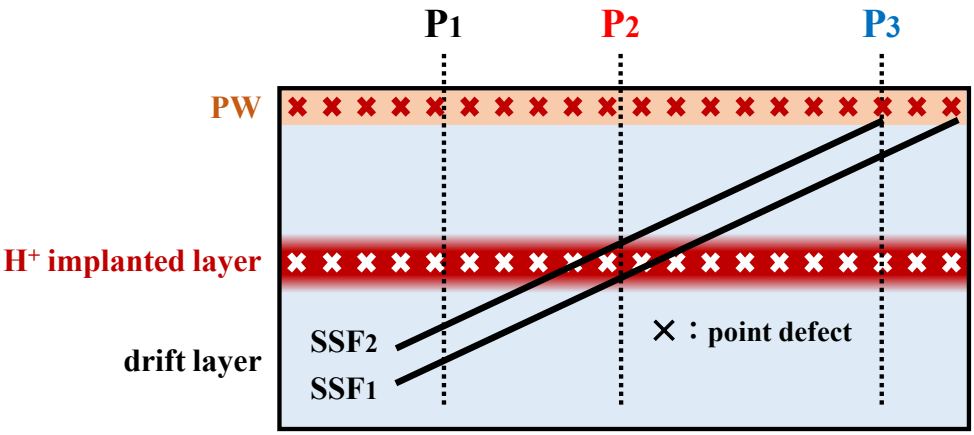

Fig. 9. Schematic diagram of the distribution of point defects introduced during the implantation process for proton-implanted SiC-MOSFET. Point defects in the drift layer are expected to exist at high densities in both the PW and the proton-implanted layer.

Summary

In this work, we have investigated the effect of proton implantation on suppressing the expansion on SSFs in SiC-MOSFETs. We fabricated a three-dimensional structure in which protons were partially implanted into the middle depth of the drift layer in SiC-MOSFET, and experimentally demonstrated how the proton-implanted layer suppresses the SSF expansion. When the expanded SSFs reached the proton-implanted region, the SSF structure remained unchanged, while the dislocation motion was hindered only in the area deeper than the proton-implanted layer. Detailed PL images and spectra of the expanded SSFs suggest that the proton-implanted layer within the drift layer can function as a recombination-enhancing layer during bipolar operation. It is inferred that the primary mechanism of degradation suppression is due to the point defects introduced by proton implantation. We believe that proton implantation allows for the formation of a recombination-enhancing layer at any depth within the drift layer by controlling the energy, offering a significant advantage in the design of SiC-MOSFETs having highly reliable body diodes.

Acknowledgement

The authors would like to thank Dr. S. Hayashi of Toray Research Center, Inc. for his technical support of TEM observation. We would also like to thank N. Kawabata, K. Miyazaki, A. Iijima, and Dr. K. Kawahara of Mitsubishi Electric for their insightful discussion and support of experiments.

References

[1] A. Galeckas, J. Linnros and P. Pirouz, Appl. Phys. Lett. **81**, 883 (2002).

[2] M. Skowronski and S. Ha, J. Appl. Phys. **99**, 011101 (2006).

[3] A. Agarwal, H. Fatima, S. Haney and S. Ryu, IEEE Electron Device Lett. **28**, 587 (2007).

[4] T. Tawara, T. Miyazawa, M. Ryo, M. Miyazato, T. Fujimoto, K. Takenaka, S. Matsunaga, M. Miyajima, A. Otsuki, Y. Yonezawa, T. Kato, H. Okumura, T. Kimoto and H. Tsuchida, J. Appl. Phys. **120**, 115101 (2016).

[5] M. Kato, O. Watanabe, T. Mii, H. Sakane and S. Harada, Sci. Rep. **12**, 18790 (2022).

[6] S. Harada, T. Mii, H. Sakane and M. Kato, Sci. Rep. **12**, 13542 (2022).

[7] A. Tanaka, H. Matsuhata, N. Kawabata, D. Mori, K. Inoue, M. Ryo, T. Fujimoto, T. Tawara, M. Miyazato, M. Miyajima, K. Fukuda, A. Ohtsuki, T. Kato, H. Tsuchida, Y. Yonezawa and T. Kimoto, J. Appl. Phys. **119**, 095711 (2016).

[8] C. Ota, J. Nishio and R. Iijima, J. Electron. Mater. **50**, 6504 (2021).

[9] A. Iijima, I. Kamata, H. Tsuchida, J. Suda and T. Kimoto, Philos. Mag. **97**, 2736 (2017).

[10] I. Kamata, X. Zhang and H. Tsuchida, Appl. Phys. Lett. **97**, 172107 (2010).

[11] N. A. Mahadik, R. E. Stahlbush, J. D. Caldwell and K. D. Hobart, Mater. Sci. Forum **717-720**, 391 (2001).

[12] T. Miyanagi, H. Tsuchida, I. Kamata, T. Nakamura, K. Nakayama, R. Ishii and Y. Sugawara, Appl. Phys. Lett. **89**, 062104 (2006).

[13] J. D. Caldwell, R. E. Stahlbush, K. D. Hobart, O. J. Glembocki and K. X. Liu, Appl. Phys. Lett. **90**, 143519 (2007).

[14] J. D. Caldwell, K. X. Liu, M. J. Tadjer, O. J. Glembocki, R. E. Stahlbush, K. D. Hobart and F. Kub, J. Electron. Mater. **36**, 318 (2007).